6-1-2007

LP133-373 A New Chromospherically Active Eclipsing dMe Binary with a Distant, Cool White Dwarf Companion

T. R. Vaccaro
Florida Institute of Technology, tvaccaro@fit.edu

T. D. Oswalt
Florida Institute of Technology, oswaltt1@erau.edu

M. Rudkin
Florida Institute of Technology, mrudkin@fit.edu

Adela Kawka
Czech Academy of Sciences, kawka@sunstel.asu.cas.cz

Stephane Vennes
Florida Institute of Technology, svennes@fit.edu

See next page for additional authors

Accepted for publication in ApJ
Preprint typeset using LaTeX style emulateapj v. 08/22/09

LP 133-373: A NEW CHROMOSPHERICALLY ACTIVE ECLIPSING dMe BINARY WITH A DISTANT, COOL WHITE DWARF COMPANION

T.R. Vaccaro[1], M. Rudkin[1], A. Kawka[2], S. Vennes[1], T.D. Oswalt[1], I. Silver[1], M. Wood[1], and J. Allyn Smith[3]

Draft version September 4, 2018

ABSTRACT

We report the discovery of the partially eclipsing binary LP 133-373. Nearly identical eclipses along with observed photometric colors and spectroscopy indicate that it is a pair of chromospherically active dM4 stars in a circular 1.6 d orbit. Light and velocity curve modeling to our differential photometry and velocity data show that each star has a mass and radius of $0.340 \pm 0.014 M_{\odot}$ and $0.33 \pm 0.02 R_{\odot}$. The binary is itself part of a common proper motion pair with LP 133-374 a cool DC or possible DA white dwarf with a mass of $0.49 - 0.82\ M_{\odot}$, which would make the system at least 3 Gyr old.

Subject headings: binaries: eclipsing — late-type — stars: activity — stars: individual (LP 133-373, LP 133-374) — white dwarfs

1. INTRODUCTION

The star LP 133-373 (NLTT 36188)—R.A.(2000)= $14^{\rm h}4^{\rm m}9^{\rm s}.0$, Dec.(2000)= $+50°20'38''$—was originally listed in the Luyten (1979) catalog as a red star ($R = 15.2$ mag) with a fainter ($R = 17.7$ mag) white dwarf star (LP 133-374, NLTT 36191) as a common-proper-motion companion separated by $5''$. Figure 1 shows a finder chart for these stars.

LP133-373 was found to be a partially eclipsing binary during unfiltered CCD-based time series photometry of the field in an attempt to detect variability of the white dwarf (Rudkin 2003; Oswalt et al. 2005). Their original estimate of the binary period (0.81 d) corresponds to half the correct period (1.63 d) because the similarity of the stellar types yields nearly identical light curves for primary and secondary eclipses. This conclusion is supported by detailed light curve modeling and the splitting of emission and well as absorption lines near quadrature. Light curve variations outside of eclipse indicate dark surface spots, which is consistent with the chromospheric activity observed in the spectra (Balmer and Ca II emissions).

Only a few eclipsing low-mass binaries in detached systems have been studied in detail. Lopez-Morales & Shaw (2006) and Shaw & Lopez-Morales (2006) report 9 such systems. Other recent identifications were made by Bayless & Orosz (2006), Hebb et al. (2006), and Young et al. (2006). Late-type M dwarf stars are prominent members of the class of eclipsing cataclysmic variables. However, the late-type star is often outshined by the white dwarf's accretion disk providing little or no mass, luminosity, or radius information crucial in understanding the physical and evolutionary nature of these stars. Reviews of late-type mass-radius relations are given by Caillault & Patterson (1990), Chabrier & Baraffe (2000), and Reid & Hawley (2000).

We present in §2 new observations of the common proper-motion pair LP 133-373/374, and, in particular, photometric and spectroscopic data confirming that LP 133-373 is itself an eclipsing late-type binary. Detailed orbital and stellar properties of the binary LP 133-373 are derived in §3.1 and an analysis of the common proper-motion companion LP 133-374 is presented in §3.2. We summarize and conclude in §4.

2. OBSERVATIONS

2.1. *Photometry*

We recently reprocessed the original photometric measurements obtained by Smith (1997) on 1994 April 2 at the Kitt Peak National Observatory (KPNO) 0.9 m telescope. See Smith (1997) for more details. We remeasured the BVRI colors for the red dwarf and white dwarf components, respectively: $B = 16.907 \pm 0.029$ mag, $V = 15.319 \pm 0.014$ mag, $R = 14.093 \pm 0.012$ mag, $I = 12.476 \pm 0.013$ mag, and $B = 18.587 \pm 0.029$ mag, $V = 18.020 \pm 0.053$ mag, $R = 17.387 \pm 0.027$ mag, $I = 16.274 \pm 0.029$ mag. The white dwarf colors were differentially determined with a field star and the red star's photometry was obtained with an aperture that excluded the white dwarf. The red dwarf data were obtained out of eclipse. The colors clearly show that the red star is approximately of dM4-5 spectral type in agreement with the spectra, which exhibit chromospheric activity and provide measurements of the TiO5 bandheads indicating a dM4 classification (see Fig. 2) in agreement with previous classifications (Silvestri et al. 2005). Our comparisons of the available colors with other dM stars in the literature (Cox 2000; Reid & Hawley 2000) also place it in the dM4 range, which we assume for our analysis.

Series of images of LP133-373 were taken with the 0.9 m telescope of the Southeastern Association for Research in Astronomy (SARA), which is also located at KPNO. The initial eclipsing data were obtained in 2003 May using SARA's Ap7P CCD and no filters. Differential light curves were produced from the 2003 through 2005 observing seasons using various comparison stars in the field. Since the data were collected and reduced by sev-

[1] Department of Physics and Space Sciences and SARA Observatory, 150 W. University Blvd, Florida Institute of Technology, Melbourne, FL 32901, USA; tvaccaro, mrudkin, svennes, toswalt, isilver, wood@fit.edu.
[2] Astronomický ústav AV ČR, Fričova 298, CZ-251 65 Ondřejov, Czech Republic; kawka@sunstel.asu.cas.cz.
[3] Department of Physics and Astronomy, Austin Peay State University, Clarksville, TN 37044 USA; smithj@apsu.edu.

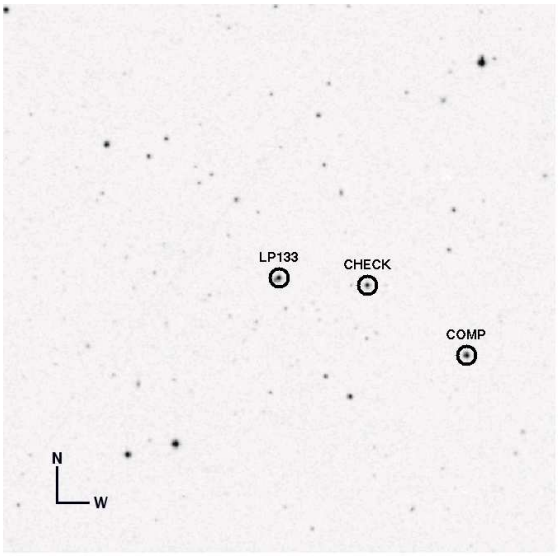

FIG. 1.— Finder chart (red POSSII) for LP133-373/374 from The STScI Digitized Sky Survey indicating by circles the binary LP133-373, the comparison, and check stars. The distant white dwarf (LP133-374) is barely visible to the southeast of the brighter binary. The image is $10' \times 10'$.

eral different observers using different comparison stars during this time and due to the unfiltered nature of the photometry, these light curves served only to establish the ephemeris. Observations made on the (UT) nights of 2006 May 2, 3, 4, 21 and 30 were taken with SARA using the Finger Lakes CCD with Johnson R and I filters. A consistent comparison was used along with a check star that was always in the field to get differential measurements. Typical exposures were 30 seconds that yielded a S/N ≈40. These stars are shown in Figure 1.

All new photometric data were reduced using standard procedures within IRAF[4] and measured with apertures a few arc seconds wide so as to exclude the white dwarf, which may have contributed less than one percent in R or I in some cases. However, we believe that observations in these pass bands for the white dwarf reported by Smith (1997) are contaminated by LP133-373; therefore, we rely on the Sloan Digital Sky Survey (SDSS) ugriz photometry for the white dwarf, which are $u = 20.018 \pm 0.038$ mag, $g = 18.797 \pm 0.008$ mag, $r = 18.256 \pm 0.007$ mag, $i = 18.004 \pm 0.009$ mag, $z = 18.076 \pm 0.020$ mag. Sloan data for the red dwarf were marked as saturated and could not be used.

Finally we obtained Two Micron All Sky Survey (Skrutskie et al. 2006, 2MASS) JHK photometry of the binary LP133-373: $J = 10.905 \pm 0.020$, $H = 10.306 \pm 0.021$, and 10.091 ± 0.015. The data are useful as an independent verification of the average M dwarf absolute luminosity. The start and end of the observations are HJD 2451322.699946 and HJD 2451322.704645, respectively, and according to our ephemeris (see §3.1 and Table 1) the data were obtained out of eclipse (phase= 0.7).

2.2. *Spectroscopy*

[4] IRAF is distributed by the National Optical Astronomy Observatories, which are operated by the Association of Universities for Research in Astronomy, Inc., under cooperative agreement with the National Science Foundation.

TABLE 1
LP133-373 PARAMETERS ($q \equiv 1.0$)

Parameter	Value
T_0	HJD 2452760.70502 ± 0.00013
P	1.6279866 ± 0.0000004 d
a	$5.10 \pm 0.22\ R_\odot$
i	$85.3 \pm 0.05°$
T_1	3058 ± 195 K
T_2	3144 ± 206 K
$M_{\rm bol,1}$	10.0 ± 0.5
$M_{\rm bol,2}$	9.8 ± 0.5
Ω_1	16.51 ± 0.12
Ω_2	16.34 ± 0.094
R_1, R_2	$0.330 \pm 0.014\ R_\odot$
M_1, M_2	$0.34 \pm 0.02\ M_\odot$

2.2.1. *KPNO 1989 February*

Spectra of the white dwarf LP133-374 and red dwarf LP133-373 were originally obtained with the Ritchey-Chrétien (RC) spectrograph attached to the 4 m telescope at KPNO on 1989 February 7 (UT). We obtained a single exposure of 1200 s with both stars on the slit. The BL250 grating (158 lines mm^{-1}) and TI-2 CCD (15 μm pixel size, circa 1989) were used to obtain a spectral range of 3500 to 6200 Å with a dispersion of 3.45 Å pixel^{-1} and a resolution of ≈ 14 Å. The resulting signal-to-noise ratio reached 15 in the red dwarf spectrum near 4150 Å, and 5 throughout the white dwarf spectrum. The white dwarf spectrum appears featureless to the noise limit. The spectrum is also relatively red indicating a low effective temperature at which hydrogen Balmer lines are expected to be weak. The white dwarf is tentatively classified as a DC. A DA classification remains possible and would be confirmed with the acquisition of a high signal-to-noise ratio Hα spectrum. The red dwarf spectrum revealed emission lines characteristic of chromospherically active stars.

2.2.2. *KPNO 2005 July*

We obtained two optical spectra of LP133-373 with exposure times of 1800 s on 2005 July 29 UT at the Mayall 4m telescope at KPNO. We used the RC spectrograph using the BL450 grating in the second order resulting in a dispersion of 0.70 Å pixel^{-1} and a resolution of 1.8 Å. The 2k×2k T2KB CCD camera with 24μm pixel size imaged the spectra. An 8-mm $CuSO_4$ order-blocking filter was used to decrease the likelihood of order overlap within the blue end of the spectrum. The range of wavelengths covered was 3800Å to 5100Å. We caught the stars near quadrature ($HJD = 2453580.67333196$ or phase= 0.67, and $HJD = 2453580.70308391$ or phase= 0.69) as predicted by the ephemeris generated from the early photometric data. Figure 2 shows prominent emission lines of H I and Ca II H and K. The Ca II H and K and the Balmer lines were split indicating a velocity separation between the two binary components of ≈ 144 km s^{-1}. Further details are presented in the analysis section (§3.1).

2.2.3. *APO 2006 September*

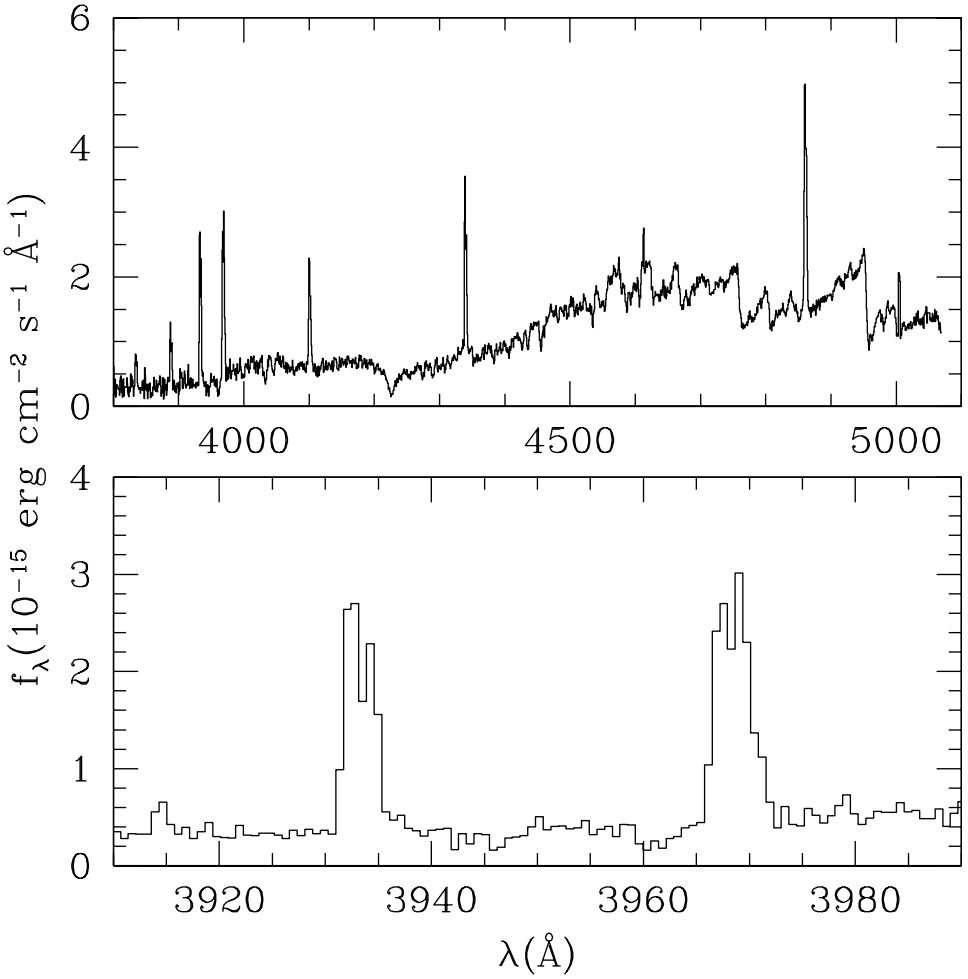

FIG. 2.— (*Top*) Mayall 4m KPNO spectrum of LP133-373 ($HJD = 2453580.703$), and (*bottom*) Ca II H and K emission lines can be seen split as the binary was near quadrature.

LP 133-373 was observed using the Dual Imaging Spectrograph (DIS) attached to the 3.5 m telescope at the Apache Point Observatory (APO) on 2006 September 30 02:31:24.7 UT and 02:47:16.0 UT (mid-exposure times). The exposure time of each spectrum is 900 s. We used the 830.8 line mm^{-1} grating to obtain a spectral range of 6440 to 8150 Å with a dispersion of 0.84 Å pixel^{-1} in the red. We also used the 1200 line mm^{-1} grating to obtain a spectral range of 3830 to 5030 Å with a dispersion of 0.62 Å pixel^{-1} to obtain a spectrum in the blue. The slit was set for 1.5" resulting in a resolution of 2.1 Å in the red and 1.7 Å in the blue. For each spectrum, the signal-to-noise ratio reached 5 near 4150 Å and 20 near Hα.

Previous spectra had been obtained at APO (Silvestri 2002; Silvestri et al. 2005) on 2001 February 4 09:59:13 UT (mid-exposure) but did not show double lines because the orbit was near conjunction (phase= 0.9). Our more recent APO spectra (2006 September 30) taken nearly an hour after eclipse (phase= 0.53) yields an Hα emission velocity $v(\mathrm{H}\alpha) = -32.0 \pm 5.0$ km s^{-1} which should closely match the systemic velocity but the expected line split (≈ 20 km s^{-1}) at this time was not detected due to limited resolution (≈ 100 km s^{-1}). Further details are presented in the analysis section (§3.1).

All new spectroscopic data were reduced using standard procedures within IRAF. Heliocentric corrections were applied to the wavelength scale of all spectra.

3. ANALYSIS

3.1. *The eclipsing binary LP 133-373*

To determine the binary parameters we followed four steps. First, we used the epoch of all seven eclipses, which include four eclipses observed using unfiltered CCD data taken during 2003-2005 and three eclipses observed using filtered photometry in 2006 May, and we determined the initial epoch of the primary mid-eclipse

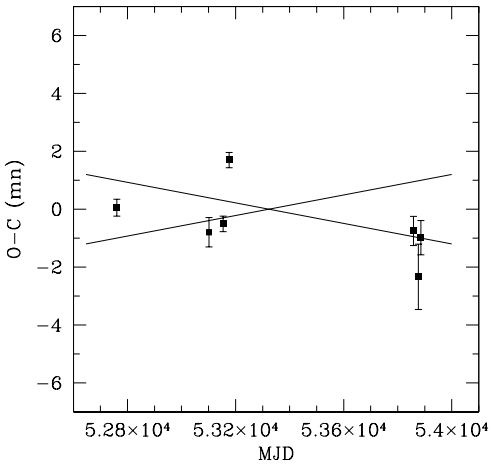

FIG. 3.— $O-C$ diagram showing deviations of the epoch measurements (in units of minutes) of seven usable eclipses relative to the adopted ephemeris versus the epoch (MJD). The full lines show expected deviations from the ephemeris if the period is increased or decreased by 5σ (0.000002 d).

and the orbital period (Table 1). Figure 3 shows the $O-C$ diagram for the epoch of all seven eclipses. Significant deviations with respect to our ephemeris are evident. We attribute these deviations to the presence of surface spots with varying contrasts and locations. The epoch of primary eclipse is (HJD)

$$T = 2452760.70502 \pm 0.00013 + E\,1.6279866 \pm 0.0000004\,\mathrm{d}$$

In a second step, we used the ephemeris as a starting point for the binary star program PHOEBE (Prša & Zwitter 2005) and we performed detailed light curve modeling of our R and I data taken in 2006 May. We do not model unfiltered data. The program PHOEBE is based on the Wilson-Devinney (WD) program (Wilson & Devinney 1971; Wilson 1979, 1990). The similarity in the primary and secondary eclipses led us to adopt a mass ratio of 1.0, a circular orbit, and typical dM4 temperatures (Cox 2000; Reid & Hawley 2000) for each star of 3100 K.

The radial velocity measurements provide the only anchor in establishing the semi-major axis a. Radial velocities were determined from our 2005 July spectroscopy, which included measurements from Hβ, Hγ, Hδ and Ca II K emission lines while excluding the very blended lines of Hϵ and Ca II H. The line centers were measured using IRAF's routine for de-blending multiple profiles, in this case two profiles—one for each star. Only 2 sets of heliocentric velocities were obtained at phase= 0.67, $v_1 = -108.2 \pm 4.4$ km s^{-1} and $v_2 = 31.1 \pm 4.1$ km s^{-1}, and phase= 0.69, $v_1 = -100.9 \pm 6.3$ km s^{-1} and $v_2 = 47.6 \pm 7.2$ km s^{-1}. The average velocity separation is 144 ± 8 km s^{-1}. A best fit to the velocities starting with the known period, a systemic velocity between the measured velocities $\approx$ -33 km s^{-1} (which is close to the APO measurement of $v = -32.0 \pm 5.0$ km s^{-1} at phase 0.53), and an inclination of 90° yields a minimum total mass of the system $\gtrsim 0.67 M_\odot$.

We repeated the radial velocity analysis using the absorption line spectra. We adopted the spectrum of the dM3.5 star Gliese 15B as a template for both component stars of LP 133-373. The spectrum of Gliese 15B was obtained at KPNO on 2006 November 27 with the same instrumental set-up used on 2005 July. We established the zero-velocity scale using the radial velocity measurement of Nidever et al. (2002), v(Gl15B) $= 11.0 \pm 0.4$ km s^{-1}. We shifted the two templates independently within a velocity range of -200 to $+200$ km s^{-1}, and fitted the combined templates to the observed spectrum of LP 133-373 using a χ^2 minimization technique. The best fits for the 2005 July spectra resulted in $v_1 = -94 \pm 10$ km s^{-1} and $v_2 = 46 \pm 10$ km s^{-1} (phase= 0.67), and $v_1 = -90 \pm 10$ km s^{-1} and $v_2 = 60 \pm 10$ km s^{-1} (phase= 0.69), which corresponds to an average velocity separation of 145 ± 14 km s^{-1}. The velocity separation measurements using absorption and emission line spectra are essentially identical. We also measured the systemic velocity in the APO 2006 September spectrum (-24 ± 7 km s^{-1}) using K I resonance lines at $\lambda = 7664.911$ and 7698.974 Å. We find that the mass ratio (M_2/M_1) ranges from ≈ 1.0 using the emission spectra to ≈ 1.1 using the absorption spectra. Although we adopted $M_2/M_1 = 1$ we will explore the effect of a varying mass ratio (see below).

Next, in a third step, the inclination and potentials (stellar radii) were then iteratively adjusted within PHOEBE until both eclipse depths and widths matched the observed light curve. Note that all solutions are based on a atmosphere of 3500 K ramped from a black body approximation at 1500 K, and on logarithmic limb darkening with coefficients by van Hamme (1993) for temperatures of 3500 K since the coefficient values are not known below this temperature. Table 1 presents the simultaneous light/velocity solutions.

Finally, in a last fourth step we introduced surface spots. Initial fits were done with the light levels adjusted to match the eclipses. We subsequently scaled the model light curve to values outside of eclipse (near phase 0.25) and spots were added to fit the complete light curve since a spot wave is clearly evident. Light curve models were compared to the eclipse geometry implied by our R, I, and unfiltered photometry. The unfiltered comparisons are only for a check on the ephemeris since spot configurations are surely different between the 2003 and 2006 epochs. We fit our photometric data with model light curves using the spot parameters given in Table 2. No satisfactory fit was possible without starspots, so cool spots were added one at a time, with typical temperature factors, $\frac{T_{spot}}{T_{photosphere}}$, of about 0.80. Spots on the facing hemisphere of each star were needed. A similar effect on the light curves would occur if the spots were on the outer facing hemispheres but the models were best fit with the inner facing configuration. The spot parameters were refined with the differential corrections routine part of the Wilson-Devinney code. Figure 4 shows the light curve using parameters for the two spots given in Table 2, and Figure 5 shows the binary configuration at four phases ($\Phi = 0.0, 0.25, 0.5, 0.75$) and as seen along the line of sight.

We also examined the sensitivity of the solutions to our our assumption of a mass ratio $q = 1$. If we let the mass ratio reach $q = 0.9$ and 1.1, in both cases the separation increases from 5.1 to 5.15 $R_\odot$ corresponding to a slight

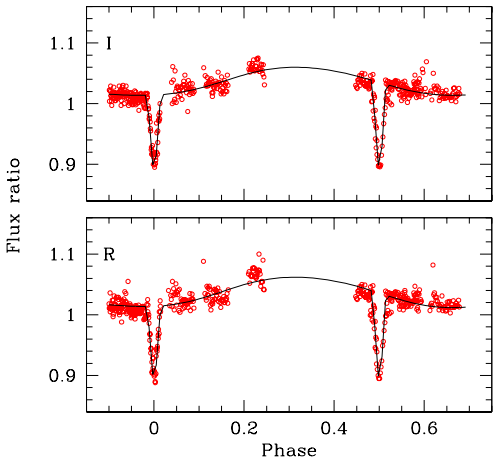

FIG. 4.— Light curve model (*solid lines*) compared with our I-band (top) and R-band (*bottom*) photometry (*open circles*).

TABLE 2
LP133-373 SPOT SOLUTIONS IN 2006 MAY DATA

Spot #	Co-Latitude (radians)	Longitude (radians)	Ang. Radius (radians)	Temp. Factor $\frac{T_{spot}}{T_{photosphere}}$
1	0.70±0.17	0.00±0.04	0.40±0.02	0.72±0.06
2	0.55±0.07	5.30±0.06	0.45±0.03	0.78±0.05

increase in the total systemic mass from 0.68 to 0.69 $M_\odot$ and no significant effect on the inclination. Of course, by introducing a mass asymmetry, the predicted systemic velocity shifts from -33 to -29 km s^{-1} at $q = 0.9$ and to -40 km s^{-1} at $q = 1.1$. The solutions closely match the limits allowed by our systemic velocity measurement of $v = -32.0 \pm 5.0$ km s^{-1}, and, therefore, the actual mass ratio should be found within the range $q = 0.9 - 1.1$.

Tables 3 and 4 present our photometry, where ΔR, ΔI refer to magnitude differences between LP133-373 and the comparison star shown in Figure 1.

3.1.1. *Luminosity and distance estimate of the red dwarf*

We computed the distance to the binary several ways. This allowed us to check the modeled binary luminosity for consistency and to find the luminosity of the white dwarf common proper motion component. Two methods of determining luminosity for the binary from observable measurements were used. One method uses the V-I colors to obtain the absolute visual magnitude M_V. The other method utilizes the TiO5 band strength to get M_V. The apparent magnitude (m_V) can then be used to compute a distance modulus. We assumed that the stars were identical enough to facilitate a simple distance correction. The inverse square law allows us to correct the distance computed for two identical stars by treating them as one and multiplying the result by $\sqrt{2}$.

The empirical color magnitude diagram of nearby stars yields the following relationship for $0.85 < V - I < 2.85$ (Reid & Hawley 2000)

$$M_V = 3.98 + 1.437\,(V-I) + 1.073\,(V-I)^2 - 0.192\,(V-I)^3,$$

with $\sigma(M_V) = 0.5$. Using our (V-I)=2.843 we get an M_V=12.3, which gives a distance of 40 pc for a single star of this color and observed $V = 15.319$. However, we correct this distance by a factor of $\sqrt{2}$ and get the distance to the system as 56 pc.

A similar relationship exists for the TiO5 band strength (Reid, Hawley & Gizis 1995),

$$M_V = 25.33 - 53.15\,(\mathrm{TiO5}) + 64.1\,(\mathrm{TiO5})^2 - 29.14\,(\mathrm{TiO5})^3,$$

with $\sigma(M_V) = 0.5$. Using TiO5= 0.37 (Silvestri 2002) we get $M_V = 13.0$ and a distance of 30 pc, which when corrected for two stars becomes 42 pc.

The PHOEBE light curve models compute bolometric magnitudes for both stars, which are similar ($M_{\rm bol} \approx 9.9 \pm 0.5$). Bolometric corrections for the visual bandpass can be computed and subtracted from the modeled $M_{\rm bol}$ to give M_V using the following relation (Reid & Hawley 2000)

$$BC_V = 0.27 - 0.604\,(V-I) - 0.125\,(V-I)^2,$$

which gives us $BC_V = 2.5$ and therefore $M_V = 12.4$ for a corrected distance of 55 pc. The model is consistent with the two independently determined distance estimates ranging from 42 to 56 pc.

In summary, the distance estimates imply a modulus of

$$m - M = 3.4 \pm 0.3$$

Adopting $m_K - M_K = 3.4 \pm 0.3$, the absolute magnitude $M_K = 6.7 \pm 0.3$ for the pair or $M_K = 7.4 \pm 0.3$ for each binary component assuming equal luminosity. The measured $V - K = 5.23 \pm 0.03$ and our M_K estimate for LP 133-373 are consistent with established relations for nearby stars (Reid & Hawley 2000). The main limitation to the usefulness of such relations is the intrinsic scatter found in color-luminosity measurements. Note that the absolute JHK magnitudes of the nearby white dwarf companion (see §3.2) are $\gtrsim 13$ mag; Therefore, potential contamination of the infrared data by the white dwarf is insignificant.

3.2. *Physical parameters and age of the white dwarf LP 133-374*

To analyze the photometric and spectroscopic data of the white dwarf LP133-374, we calculated a set of synthetic SDSS *ugriz* colors using a grid of pure-hydrogen models (Kawka & Vennes 2006) for $T_{\rm eff} = 4500$ to 84 000 K and $\log g = 7.0$, 8.0 and 9.0. We also calculated synthetic *ugriz* colors for black-body spectra with temperatures ranging from $T_{\rm eff} = 4500$ to 84 000 K. Figures 6 and 7 show the observed $(u-g)$ versus $(g-r)$ and $(r-i)$ versus $(g-r)$ colors, respectively, compared to the synthetic colors for pure-hydrogen models and the black-body colors.

Note that Kowalski & Saumon (2006) recently established that the extended line wing of Lyα contributes significantly to the total opacity in the blue part of the optical spectrum. The additional opacity is due to perturbation of the hydrogen atom by neighboring H atoms

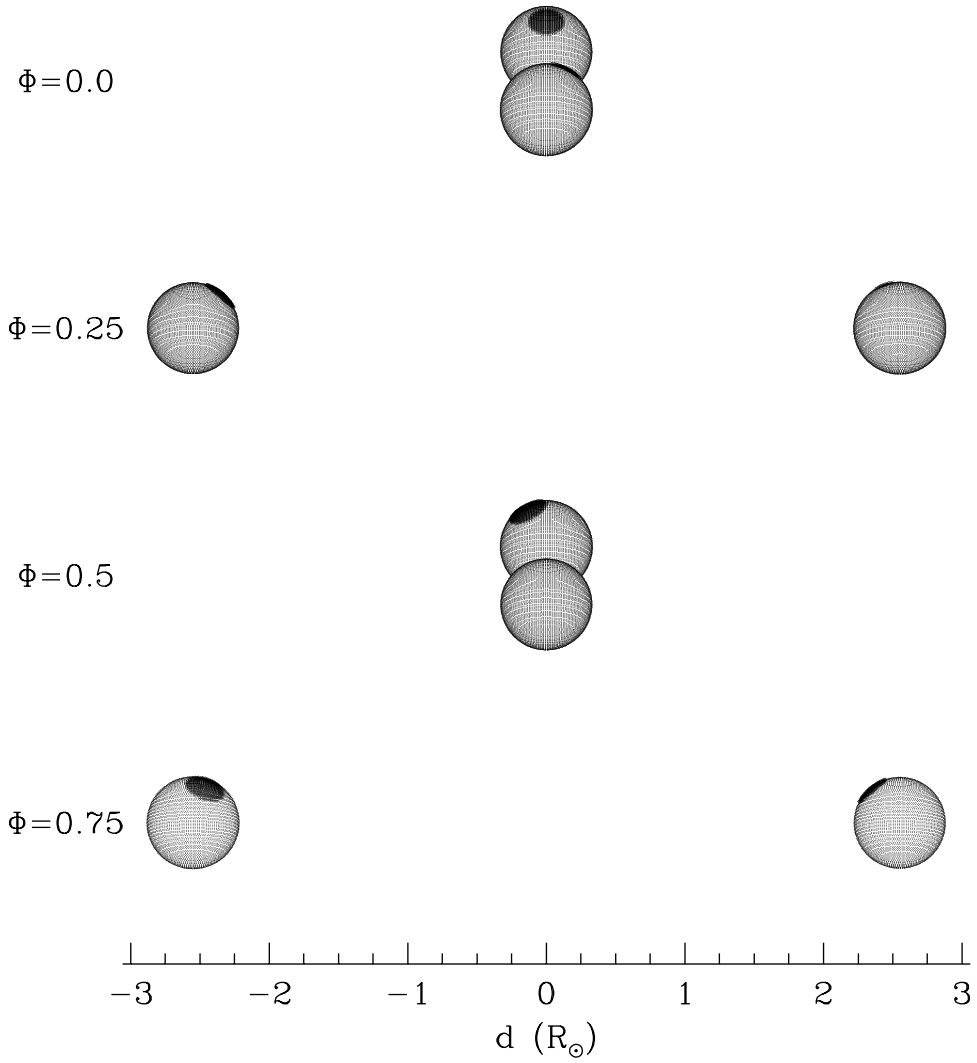

FIG. 5.— Binary configuration as seen along the line of sight at $\Phi = 0.0, 0.25$, and 0.5. The images were generated with PHOEBE.

and H_2 molecules. An examination of Figure 2 in Kowalski & Saumon (2006) suggests that the effect of this additional opacity on a 5800 K hydrogen-rich white dwarf corresponds to an increase of ≈ 0.25 and 0.02 mag in the u and g bands, respectively. Hence, the effect is mostly apparent in the $u-g$ color index and correspond, as observed, to a downward vertical shift in the $u-g$ versus $g-r$ diagram.

The temperatures were derived by minimizing the χ^2 between the observed photometry and the synthetic colors. The synthetic u and g magnitudes for hydrogen-rich models were corrected by +0.25 and +0.02 mag, respectively. The errors in temperatures were determined from considering the uncertainties in the observed colors only. Therefore, the quoted errors do not take into account systematic errors in synthetic colors such as discussed above. The observed $(u-g)$ versus $(g-r)$ colors correspond to an effective temperature of 5200 ± 100 K using the pure-hydrogen sequence, and 5300 ± 100 K using the black-body colors. The observed $(r-i)$ versus $(g-r)$ colors correspond to an effective temperature of 5100 ± 100 K using the pure-hydrogen sequence and 5400 ± 50 K using black-body colors.

We also fit the SDSS *ugriz* photometry to synthetic *ugriz* absolute magnitudes, and found that $T_{\rm eff} = 5300 \pm 200$ K when using the hydrogen-rich sequence (assuming $\log g = 8.0$) and $T_{\rm eff} = 5500 \pm 200$ K assuming a black-body. We also fit the available spectrum (3800 to 6190 Å) to DA spectra at $\log g = 8.0$ and black-body spectra to obtain $T_{\rm eff} = 5100 \pm 200$ K and $T_{\rm eff} = 5580 \pm 160$ K, respectively. Figure 8 shows the spectrum and *ugriz* photometry of LP133-374 compared to a hydrogen-rich spectrum at $T_{\rm eff} = 5100$ K and a blackbody spectrum at $T_{\rm eff} = 5500$ K.

We determined the possible range of mass values for the white dwarf assuming both hydrogen-rich atmospheres and helium-rich atmospheres (using a black-body approximation). First, we calculated the absolute mag-

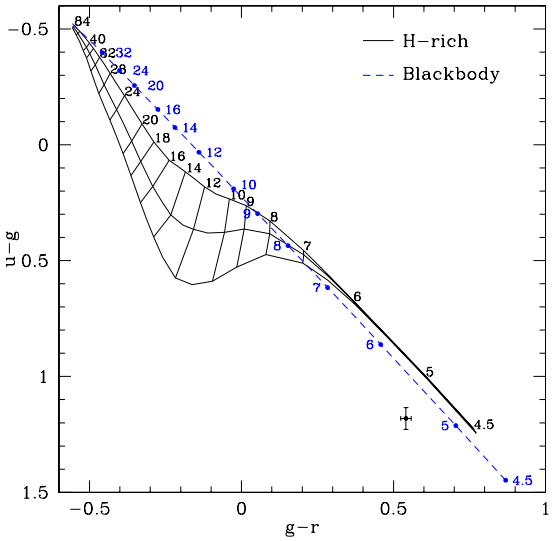

FIG. 6.— SDSS $(u-g)$ vs. $(g-r)$ photometry of LP133-374 (*full circle* with error bars) compared to synthetic colors of hydrogen-rich white dwarfs (*full line*) and blackbody (*dotted line*). The effective temperature is indicated in units of 1000 K and for hydrogen-rich colors $\log g = 7.0$, 8.0 and 9.0 (*bottom to top*). The grid shown does not include the effect of missing blue/ultraviolet opacity.

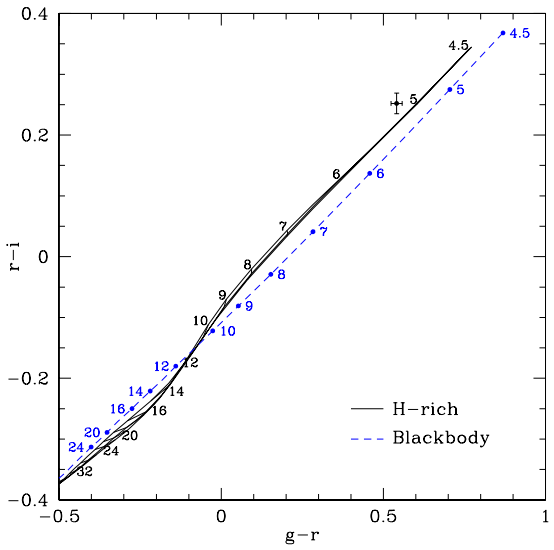

FIG. 7.— SDSS $(r-i)$ vs. $(g-r)$ photometry of LP133-374 compared (*full circle* and error bars) to synthetic colors of hydrogen-rich white dwarfs (*full line*) and blackbody (*dotted line*). The effective temperature is indicated in units of 1000 K and for hydrogen-rich colors $\log g = 7.0$, 8.0 and 9.0 (*bottom to top*).

nitude of the white dwarf based on the distance, and therefore if the system is between 42 and 56 pc, then the absolute magnitude (M_g) of the white dwarf is between 15.68 and 15.06.

Assuming the white dwarf is hydrogen-rich, then the mean of the temperatures determined above is $T_{\rm eff} = 5175 \pm 100$ K. The mass range can then be determined using the mass-radius relations of Benvenuto & Althaus (1999) with a hydrogen envelope of $M_H/M_\star = 10^{-4}$ and a metallicity of $Z = 0$, where for a given temperature, the absolute magnitude is a function of the radius and therefore the mass. We determined a mass of $0.49 - 0.70\ M_\odot$ with a cooling age ranging from 3.6×10^9 to 4.5×10^9 years.

Assuming the white dwarf is helium-rich, and using a black-body approximation for the energy distribution, then the mean of the temperatures determined using the different methods as discussed above is $T_{\rm eff} = 5445 \pm 120$ K. For the mass determinations in this case, we used the mass-radius relations of Benvenuto & Althaus (1999) without a hydrogen envelope and with a metallicity of $Z = 0.001$. Therefore, if LP133-374 is a helium-rich white dwarf with $T_{\rm eff} = 5445$ K, we can estimate the mass to be between 0.55 and $0.82 M_\odot$ and the cooling age to be between 2.7×10^9 and 4.5×10^9 years. The progenitor of a $0.82\ M_\odot$ white dwarf is a early-type star of $\approx 4\ M_\odot$ (Weidemann 2000) with a main-sequence lifetime $\approx 10^8$ years. These ages imply a minimum age of 3×10^9 years for the LP133-373/374 system.

For a temperature range of 5000-5500 K, the corresponding 2MASS absolute magnitude $M_J = 13.4 - 13.6$, or an apparent magnitude of $m_J = 16.5 - 16.7$, fainter than the limiting magnitude of the 2MASS survey.

4. SUMMARY AND CONCLUSIONS

We have modeled light and velocity curves of LP133-373 as an eclipsing binary with two similar dM type stars with spots. Although the masses and radii of $0.340 \pm 0.014 M_\odot$ and $0.33 \pm 0.02 R_\odot$ make them appear marginally more massive and smaller than other stars of the same type tabulated by Reid & Hawley (2000), a complete radial velocity study and additional light curves are required before we can reach a conclusion on this matter. The uncertainty in the mass ratio and the paucity of velocity data create a large uncertainty in the semi-major axis and ultimately in the individual masses. The role of spots also play a critical role in light curve modeling and the resulting fits. The 2006 May data set shows light curve variations suggesting that spot activity had significantly changed within a month. We intend on obtaining high-dispersion spectra of LP133-374 sampling a complete orbital period in the Hα region. New photometry, covering several complete orbital periods, would be helpful in constraining the geometry of the spots and the individual temperatures. The new data will provide better mass, luminosity, and radius information that is so important for understanding low mass stars. In addition, limb darkening of these cool stars is also important to the light curve models. A study of additional stars like these is needed to refine limb darkening models.

The white dwarf is tentatively classified as a DC spectral type, and a possible DA type. It has a temperature of 5100 to 5500 K depending on the atmospheric abundance of hydrogen. Adopting the distance of its common proper-motion companion LP133-373 (42-56 pc) we constrain the radius, hence the mass of the white dwarf. The mass of the white dwarf is estimated to be $0.49 \lesssim M/M_\odot \lesssim 0.82$. Consequently, the minimum total age of the system is 3 Gyr. The angular separation of $5''$ between the white dwarf and the eclipsing binary corresponds to a projected separation of 210-280 AU. This separation excludes the possibility of past interactions.

New Hα spectroscopy will also help establish the spectral type of the white dwarf, and accurately determine its physical characteristics. In turn, this will be helpful in establishing the age of the triple system from the white

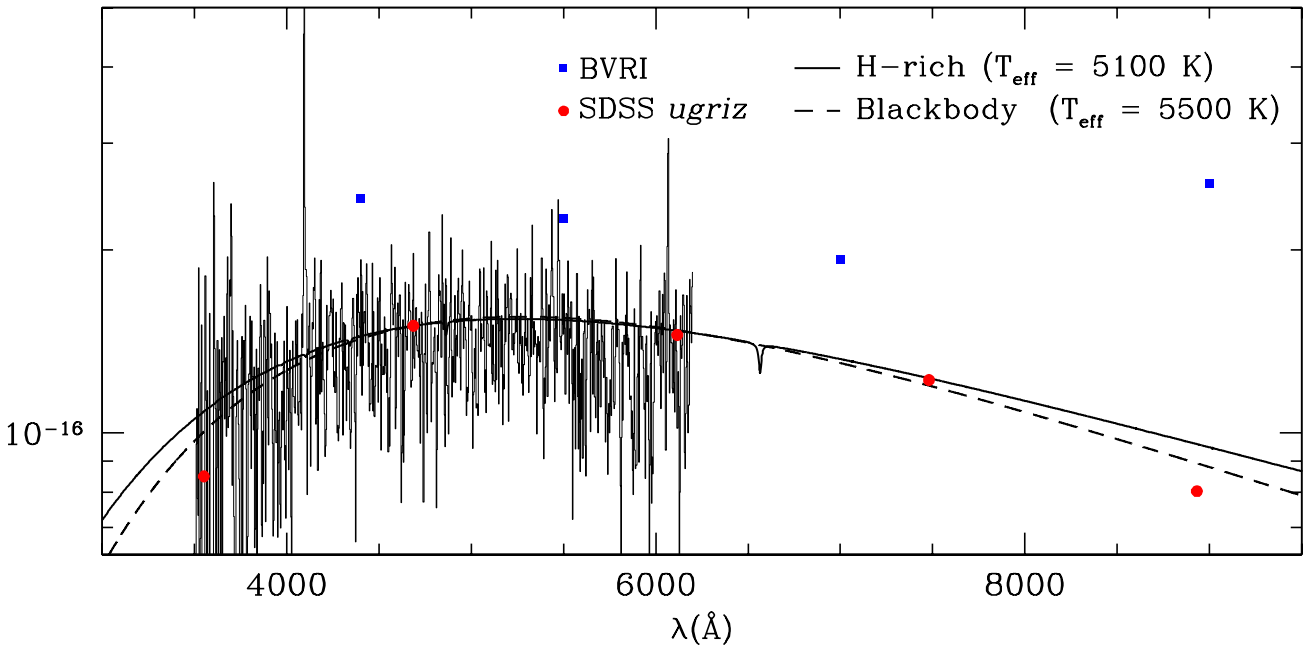

FIG. 8.— SDSS *ugriz* and *BVRI* photometry and a spectrum of LP133-374 compared to a model DA spectrum and a black-body spectrum. The hydrogen model shown does not include the effect of missing blue/ultraviolet opacity.

dwarf cooling age.

We thank KPNO for a generous allocation of observing time. We are especially grateful for the observing support of Rob Wilkos, John Robertson, and Kyle Johnston. M.R. is supported by a NASA Graduate Student Research Program NGT5-50450. A. Kawka is supported by GA ČR 205/05/P186. S.V. acknowledges support from the College of Science at the Florida Institute of Technology. This work was supported in part by NSF grant AST-0206115 (T. D. Oswalt Principal Investigator) to Florida Institute of Technology. M.W. acknowledges support from a NSF grant AST-0097616. We thank S. Shaw, R. Wilson, and Casey T. Hendley for useful discussions and N. Silvestri for sharing observing time at APO. We thank the anonymous referee for several useful comments that improved the paper.

This research is also based in part on observations obtained with the Apache Point Observatory 3.5-meter telescope, which is owned and operated by the Astrophysical Research Consortium (ARC). Funding for the SDSS and SDSS-II has been provided by the Alfred P. Sloan Foundation, the Participating Institutions, the National Science Foundation, the U.S. Department of Energy, the National Aeronautics and Space Administration, the Japanese Monbukagakusho, the Max Planck Society, and the Higher Education Funding Council for England. The SDSS Web Site is http://www.sdss.org/. This publication also makes use of data products from the Two Micron All Sky Survey, which is a joint project of the University of Massachusetts and the Infrared Processing and Analysis Center/California Institute of Technology, funded by the National Aeronautics and Space Administration and the National Science Foundation.

REFERENCES

Bayless, A. J., & Orosz, J. A. 2006, ApJ, 651, 1155
Benvenuto, O.G. & Althaus, L.G. 1999, MNRAS, 303, 30
Caillault, J.-P., & Patterson, J. 1990, AJ, 100, 825
Chabrier, G., & Baraffe, I. 2000, ARA&A, 38, 337
Cox, A. N. 2000, Allen's astrophysical quantities, 4th ed. Publisher: New York: AIP Press; Springer, 2000. Edited by Arthur N. Cox, p. 388
Hebb, L., Wyse, R. F. G., Gilmore, G., & Holtzman, J. 2006, AJ, 131, 555
Kawka, A. & Vennes, S. 2006, ApJ, 643, 402
Kowalski, P.M., & Saumon. D. 2006, ApJ, 651, L137
Lopez-Morales, M., & Shaw, J. S. 2006, ArXiv Astrophysics e-prints, arXiv:astro-ph/0603748
Luyten, W. J. 1979, A catalogue of stars with proper motions exceeding 0.″5 annually, Minneapolis: University of Minnesota, 1979, 2nd ed.
Nidever, D. L., Marcy, G. W., Butler, R. P., Fischer, D. A., & Vogt, S. S. 2002, ApJS, 141, 503
Oswalt, T. D., Rudkin, M., Johnston, K., Kissinger, J., & Menezes, K. 2005, ASP Conf. Ser. 334: 14th European Workshop on White Dwarfs, 334, 605
Prša, A., & Zwitter, T. 2005, ApJ, 628, 426
Reid, N., & Hawley, S. L. 2000, New light on dark stars : red dwarfs, low mass stars, brown dwarfs, New York : Springer
Reid, N., Hawley, S. L., & Gizis, J. E. 1995, AJ, 110, 1838
Rudkin, M. 2003, Florida Institute of Technology, M.Sc. Thesis
Shaw, J. S., & Lopez-Morales, M. 2006, ArXiv Astrophysics e-prints, arXiv:astro-ph/0603744
Silvestri, N. M. 2002, Florida Institute of Technology, Ph.D. Thesis
Silvestri, N. M., Hawley, S. L., & Oswalt, T. D. 2005, AJ, 129, 2428
Smith, J.A. 1997, Florida Institute of Technology, Ph.D. Thesis
Skrutskie, M.F. et al. 2006, AJ, 131, 1163
van Hamme, W. 1993, AJ, 106, 2096
Young, T. B., Hidas, M. G., Webb, J. K., Ashley, M. C. B., Christiansen, J. L., Derekas, A., & Nutto, C. 2006, MNRAS, 370, 1529
Weidemann, V. 2000, A&A, 363, 647
Wilson R.E. 1979, ApJ, 234, 1054
Wilson R.E. 1990, ApJ, 356, 613
Wilson R.E., Devinney, E.J. 1971, ApJ, 166, 605

TABLE 3
PHOTOMETRIC R DATA FOR LP133-373

HJD -2453800	ΔR	HJD -2453800	ΔR	HJD -2453800	ΔR	HJD -2453800	ΔR	HJD -2453800	ΔR
57.74370	-0.024	57.86909	-0.005	58.70187	-0.027	59.67035	-0.037	59.98506	-0.058
57.74743	-0.004	57.86968	-0.018	58.70397	-0.042	59.67243	-0.035	59.98715	-0.057
57.74804	-0.012	57.87225	-0.009	58.70605	-0.037	59.67451	-0.054	59.98923	-0.094
57.74863	-0.016	57.87284	-0.014	58.70816	-0.043	59.67660	-0.017	59.99132	-0.045
57.75122	-0.015	57.87343	-0.058	58.71025	-0.049	59.67869	-0.039	59.99341	-0.044
57.75182	-0.018	57.87600	-0.006	58.71235	-0.032	59.68079	-0.035	76.65658	0.001
57.75241	-0.013	57.87659	-0.010	58.71443	-0.040	59.68287	-0.043	76.65862	-0.008
57.75499	-0.024	57.87718	-0.016	58.71653	-0.049	59.68495	-0.008	76.66048	0.000
57.75559	0.003	57.87975	-0.005	58.71862	-0.053	59.68705	-0.045	76.66320	0.010
57.75618	-0.018	57.88034	-0.019	58.72072	-0.036	59.68913	-0.004	76.66591	-0.003
57.75877	0.005	57.88093	-0.016	58.72281	-0.040	59.69123	-0.018	76.66863	0.013
57.75938	-0.014	57.88354	-0.011	58.72491	-0.036	59.69331	-0.028	76.67134	0.025
57.75998	-0.020	57.88414	-0.008	58.72700	-0.034	59.69539	-0.020	76.67406	0.060
57.76255	-0.015	57.88473	0.005	58.72910	-0.052	59.69747	-0.025	76.67678	0.063
57.76314	0.005	57.88732	0.002	58.73119	-0.031	59.69956	-0.011	76.67951	0.092
57.76374	-0.010	57.88792	-0.009	58.73329	-0.031	59.70165	-0.026	76.68222	0.102
57.76630	-0.027	57.88853	-0.001	58.73537	-0.035	59.70375	-0.027	76.68494	0.114
57.76689	-0.005	57.89112	-0.012	58.73746	-0.040	59.70584	-0.013	76.68766	0.120
57.76749	-0.022	57.89171	-0.002	58.73956	-0.032	59.70793	-0.027	76.69039	0.120
57.77005	-0.017	57.89231	-0.011	58.74165	-0.030	59.71002	-0.023	76.69312	0.110
57.77064	-0.023	57.89490	-0.006	58.74375	-0.026	59.71212	-0.024	76.69584	0.098
57.77124	-0.024	57.89550	-0.001	58.74583	-0.028	59.71420	-0.018	76.69856	0.086
57.77383	-0.024	57.89611	-0.008	58.74793	-0.038	59.71629	-0.023	76.70128	0.057
57.77443	-0.022	57.89870	0.008	58.75002	-0.049	59.71837	-0.013	76.70400	0.049
57.77504	-0.014	57.89929	0.001	58.75212	-0.038	59.72045	-0.026	76.70672	0.029
57.77763	-0.025	57.89989	-0.016	58.75421	-0.039	59.72254	-0.023	76.70944	0.014
57.77822	-0.024	57.90248	-0.003	58.75632	-0.040	59.72463	-0.037	76.71216	0.002
57.77882	-0.023	57.90309	-0.013	58.75841	-0.051	59.72672	-0.008	76.71488	0.002
57.78141	-0.023	57.90369	-0.015	58.76051	-0.017	59.72880	-0.025	76.71760	-0.002
57.78200	-0.015	57.90628	-0.004	58.76260	-0.014	59.73090	-0.028	76.72033	-0.008
57.78260	-0.025	57.90688	-0.011	58.76468	-0.011	59.73299	-0.036	76.72665	-0.002
57.78520	-0.019	57.90747	-0.002	58.76678	0.012	59.73508	-0.028	76.73270	-0.004
57.78580	-0.036	57.91008	-0.006	58.76889	0.041	59.73718	-0.024	76.76273	-0.010
57.78639	-0.032	57.91068	-0.005	58.77098	0.044	59.73928	-0.012	76.76536	-0.023
57.78895	-0.027	57.91128	-0.017	58.77307	0.068	59.77400	-0.092	76.76809	-0.016
57.78954	-0.017	57.91386	-0.009	58.80441	-0.042	59.77940	-0.037	76.77079	-0.015
57.79014	-0.012	57.91446	-0.012	58.80650	-0.035	59.78218	-0.030	76.77348	-0.016
57.79273	-0.027	57.91506	-0.003	58.80859	-0.020	59.78426	-0.026	76.77619	-0.009
57.79332	-0.033	57.91766	-0.002	58.81069	-0.039	59.78636	-0.050	76.77891	-0.016
57.79392	-0.029	57.91826	-0.005	58.81278	-0.033	59.78844	-0.035	76.78164	-0.043
57.79653	-0.028	57.91885	-0.012	58.81488	-0.031	59.79054	-0.047	76.78436	-0.026
57.79713	-0.027	57.92145	-0.006	58.81697	-0.038	59.79263	-0.034	76.78707	-0.014
57.79772	-0.029	57.92204	-0.003	58.81908	-0.035	59.79472	-0.050	76.78979	-0.015
57.80032	-0.008	57.92264	-0.014	58.82118	-0.028	59.79680	-0.045	76.79250	-0.029
57.80091	-0.025	57.92643	-0.015	58.82327	-0.031	59.79889	-0.017	76.79523	-0.016
57.80152	-0.012	57.92903	-0.013	58.82536	-0.026	59.80099	-0.009	76.79794	-0.022
57.80411	0.007	57.92962	-0.013	58.82746	-0.024	59.80308	-0.020	76.80068	-0.024
57.80471	-0.019	57.93021	0.009	58.82954	-0.037	59.80516	-0.027	76.80340	-0.015
57.80531	-0.012	57.93278	-0.011	58.83164	-0.034	59.80723	-0.019	76.80612	-0.023
57.80789	-0.011	57.93339	0.008	58.83374	-0.033	59.80930	-0.025	76.80884	-0.020
57.80850	-0.038	57.93399	0.005	58.83581	-0.035	59.81138	-0.040	76.81156	-0.025
57.80910	-0.005	57.93658	0.005	58.83791	-0.038	59.81347	-0.045	76.81427	-0.024
57.81170	-0.012	57.93717	0.002	58.84001	-0.040	59.81556	-0.028	76.81699	-0.024
57.81230	-0.014	57.93777	0.005	58.84210	-0.030	59.81765	-0.044	76.81971	-0.025
57.81289	-0.018	57.94036	0.001	58.84421	-0.037	59.81975	-0.043	76.82243	-0.026
57.81549	-0.012	57.94095	-0.018	58.84630	-0.031	59.82183	-0.033	76.82515	-0.010
57.81609	-0.009	57.94156	0.000	58.84840	-0.039	59.82393	-0.039	76.82788	-0.013
57.81669	-0.026	57.94415	-0.027	58.85049	-0.026	59.82601	-0.047	76.83060	-0.006
57.81929	0.003	57.94475	-0.005	58.85258	-0.026	59.82810	-0.024	76.87240	-0.008
57.81988	-0.001	57.94534	-0.017	58.85469	-0.015	59.83020	-0.029	76.87515	-0.017
57.82049	-0.026	57.94793	0.005	58.85679	-0.031	59.83228	-0.040	76.87787	-0.020
57.82308	-0.033	57.94853	0.000	58.85888	-0.034	59.83437	-0.022	76.88057	-0.015
57.82367	-0.018	57.94914	0.015	58.86098	-0.034	59.83645	-0.013	76.88331	-0.086
57.82426	-0.012	57.95173	0.047	58.86307	-0.023	59.83853	-0.026	76.88603	-0.035
57.82685	-0.016	57.95233	0.034	58.86516	-0.037	59.84063	-0.027	76.88876	-0.038
57.82745	-0.018	57.95292	0.036	58.86725	-0.031	59.84271	-0.024	76.89148	-0.031
57.82804	-0.011	57.95551	0.071	58.86934	-0.020	59.84479	-0.026	76.89421	-0.025
57.83064	-0.008	57.95610	0.063	58.87145	-0.031	59.84689	-0.032	76.89693	-0.031
57.83124	-0.031	57.95671	0.061	58.87354	-0.039	59.84898	-0.022	76.89966	-0.024
57.83183	-0.013	57.95930	0.088	58.87565	-0.028	59.85107	-0.022	76.90238	-0.018
57.83442	-0.030	57.95990	0.107	58.87775	-0.032	59.85315	-0.028	76.90511	-0.009
57.83502	-0.011	57.96050	0.110	58.87984	-0.023	59.85523	-0.026	76.90783	-0.016
57.83561	-0.015	57.96308	0.080	58.88192	-0.025	59.85733	-0.029	76.91055	-0.014
57.83820	-0.031	57.96368	0.100	58.88403	-0.026	59.85941	-0.037	76.91328	-0.018

TABLE 3 — *Continued*

HJD -2453800	ΔR	HJD -2453800	ΔR	HJD -2453800	ΔR	HJD -2453800	ΔR	HJD -2453800	ΔR
57.83881	-0.027	57.96429	0.081	58.88613	-0.026	59.86149	-0.020	76.91600	-0.033
57.83941	-0.004	57.96688	0.106	58.90394	-0.020	59.86358	-0.044	76.91872	-0.008
57.84199	-0.015	57.96747	0.105	58.90603	-0.038	59.93702	-0.070	76.92144	-0.012
57.84259	0.000	57.96807	0.116	58.90813	-0.034	59.93912	-0.074	76.92416	-0.014
57.84319	-0.004	57.97066	0.113	58.91023	-0.050	59.94122	-0.055	76.92689	-0.014
57.84580	-0.008	57.97126	0.127	58.91233	-0.035	59.94537	-0.067	76.92961	-0.006
57.84639	-0.012	57.97187	0.129	58.91442	-0.031	59.94745	-0.066	76.93233	-0.009
57.84699	-0.016	57.97446	0.111	58.91652	-0.025	59.94955	-0.068	76.93506	-0.023
57.84958	-0.011	57.97506	0.076	58.91862	-0.038	59.95163	-0.081	76.93778	-0.013
57.85018	0.013	57.97565	0.064	58.92072	-0.037	59.95371	-0.075	76.94049	-0.022
57.85078	-0.026	57.97823	0.067	58.92490	-0.036	59.95581	-0.081	76.94318	-0.024
57.85338	-0.005	57.97882	0.061	58.92699	-0.044	59.95790	-0.081	76.94586	-0.003
57.85397	-0.006	57.97943	0.058	58.92908	-0.022	59.95999	-0.066	76.94859	-0.013
57.85457	-0.024	57.98199	0.038	58.93117	-0.027	59.96207	-0.065	76.95131	-0.018
57.85716	-0.015	57.98258	0.043	58.93327	-0.024	59.96416	-0.063	76.95403	-0.013
57.85776	-0.020	57.98318	0.026	59.64748	-0.043	59.96625	-0.066	76.95675	-0.025
57.85837	-0.028	57.98577	0.034	59.65218	-0.016	59.96833	-0.075	76.95947	-0.013
57.86096	-0.016	57.98636	-0.005	59.65572	-0.034	59.97043	-0.072	76.96218	-0.014
57.86155	-0.040	57.98696	0.004	59.65781	-0.027	59.97251	-0.078	76.96490	-0.016
57.86215	-0.016	57.98955	-0.025	59.65990	-0.015	59.97461	-0.103	76.96762	-0.020
57.86474	-0.023	57.99014	-0.015	59.66198	-0.058	59.97670	-0.076	76.97035	-0.016
57.86534	-0.037	57.99074	-0.005	59.66407	-0.034	59.97879	-0.070	76.97307	-0.016
57.86594	-0.024	58.69591	-0.032	59.66617	-0.046	59.98088	-0.050	76.97579	-0.026
57.86850	-0.002	58.69978	-0.029	59.66826	-0.009	59.98296	-0.057	76.97852	-0.014

TABLE 4
PHOTOMETRIC I DATA FOR LP133-373

HJD -2453800	ΔI	HJD -2453800	ΔI	HJD -2453800	ΔI	HJD -2453800	ΔI	HJD -2453800	ΔI
57.74927	-0.010	57.87407	-0.018	58.70605	-0.037	59.66716	-0.003	59.97978	-0.060
57.74988	-0.010	57.87467	-0.009	58.70816	-0.043	59.66925	-0.008	59.98186	-0.068
57.75048	-0.030	57.87526	0.003	58.71025	-0.049	59.67134	-0.057	59.98396	-0.067
57.75305	-0.030	57.87782	-0.001	58.71235	-0.032	59.67341	-0.022	59.98605	-0.058
57.75364	-0.011	57.87842	-0.019	58.71443	-0.040	59.67551	-0.002	59.98813	-0.052
57.75424	-0.008	57.87901	-0.005	58.71653	-0.049	59.67759	-0.028	59.99022	-0.067
57.75683	-0.013	57.88158	-0.013	58.71862	-0.053	59.67969	-0.031	59.99231	-0.047
57.75803	-0.015	57.88218	-0.018	58.72072	-0.036	59.68178	-0.012	59.99441	-0.033
57.76063	-0.003	57.88279	-0.008	58.72281	-0.040	59.68387	-0.029	76.66179	-0.003
57.76122	-0.024	57.88538	-0.019	58.72491	-0.036	59.68595	-0.024	76.66451	-0.004
57.76181	-0.009	57.88598	-0.003	58.72700	-0.034	59.68803	-0.025	76.66720	0.013
57.76438	-0.012	57.88657	-0.001	58.72910	-0.052	59.69013	-0.015	76.66993	0.026
57.76497	-0.031	57.88917	-0.010	58.73119	-0.031	59.69221	-0.029	76.67264	0.032
57.76556	-0.022	57.88978	0.001	58.73329	-0.031	59.69429	-0.029	76.67537	0.065
57.76813	0.007	57.89037	0.002	58.73537	-0.035	59.69638	-0.008	76.67808	0.082
57.76872	-0.005	57.89296	-0.008	58.73746	-0.040	59.69847	-0.024	76.68082	0.095
57.76931	-0.003	57.89356	-0.016	58.73956	-0.032	59.70055	-0.033	76.68352	0.105
57.77249	-0.002	57.89415	-0.012	58.74165	-0.030	59.70265	-0.039	76.68624	0.118
57.77308	-0.014	57.89676	-0.010	58.74375	-0.026	59.70474	-0.033	76.68897	0.116
57.77567	-0.015	57.89734	-0.023	58.74583	-0.028	59.70684	-0.050	76.69170	0.119
57.77627	0.000	57.89795	-0.012	58.74793	-0.038	59.70892	-0.029	76.69443	0.116
57.77688	0.003	57.90054	-0.001	58.75002	-0.049	59.71102	-0.028	76.69715	0.096
57.77947	-0.015	57.90114	0.002	58.75212	-0.038	59.71311	-0.019	76.69987	0.079
57.78006	-0.024	57.90173	-0.020	58.75421	-0.039	59.71519	-0.031	76.70259	0.061
57.78066	-0.028	57.90434	-0.010	58.75632	-0.040	59.71728	0.014	76.70530	0.036
57.78325	-0.024	57.90494	-0.016	58.75841	-0.051	59.71935	-0.040	76.70803	0.020
57.78384	-0.017	57.90553	-0.004	58.76051	-0.017	59.72144	-0.027	76.71073	0.008
57.78444	-0.034	57.90812	-0.001	58.76260	-0.014	59.72354	-0.016	76.71346	-0.009
57.78703	-0.006	57.90872	-0.014	58.76468	-0.011	59.72562	-0.035	76.71618	-0.004
57.78762	-0.017	57.90932	-0.002	58.76678	0.012	59.72772	-0.025	76.71890	-0.006
57.78822	-0.018	57.91193	-0.002	58.76889	0.041	59.72980	-0.019	76.72163	-0.015
57.79079	-0.030	57.91252	0.012	58.77098	0.044	59.73190	-0.026	76.72795	-0.001
57.79139	-0.028	57.91312	-0.011	58.77307	0.068	59.73399	-0.035	76.73401	0.002
57.79198	-0.003	57.91571	-0.013	58.80441	-0.042	59.73607	-0.018	76.76668	-0.015
57.79457	-0.019	57.91630	-0.016	58.80650	-0.035	59.73817	-0.026	76.76939	-0.005
57.79517	-0.002	57.91690	-0.008	58.80859	-0.020	59.74026	-0.022	76.77208	-0.016
57.79576	-0.016	57.91950	-0.010	58.81069	-0.039	59.77498	-0.062	76.77478	-0.024
57.79837	-0.020	57.92010	-0.018	58.81278	-0.033	59.78040	-0.049	76.77750	-0.010
57.79896	-0.030	57.92070	-0.016	58.81488	-0.031	59.78318	-0.031	76.78022	-0.013
57.79956	-0.006	57.92329	-0.005	58.81697	-0.038	59.78526	-0.034	76.78295	-0.028

TABLE 4 — *Continued*

HJD -2453800	ΔI	HJD -2453800	ΔI	HJD -2453800	ΔI	HJD -2453800	ΔI	HJD -2453800	ΔI
57.80216	-0.017	57.92388	-0.014	58.81908	-0.035	59.78734	-0.046	76.78566	-0.027
57.80277	-0.017	57.92448	-0.013	58.82118	-0.028	59.78944	-0.031	76.78838	-0.017
57.80336	-0.018	57.92708	-0.006	58.82327	-0.031	59.79153	-0.032	76.79109	-0.002
57.80595	-0.024	57.92768	-0.005	58.82536	-0.026	59.79362	-0.038	76.79382	-0.019
57.80655	-0.004	57.92828	0.001	58.82746	-0.024	59.79571	-0.037	76.79653	-0.010
57.80715	-0.024	57.93086	-0.012	58.82954	-0.037	59.79779	-0.042	76.79925	-0.015
57.80975	-0.022	57.93145	0.004	58.83164	-0.034	59.79989	-0.035	76.80199	-0.017
57.81035	-0.031	57.93204	0.008	58.83374	-0.033	59.80198	-0.044	76.80471	-0.015
57.81095	-0.014	57.93462	-0.008	58.83581	-0.035	59.80407	-0.019	76.80743	-0.018
57.81354	-0.012	57.93523	-0.018	58.83791	-0.038	59.80614	-0.013	76.81015	-0.024
57.81414	-0.004	57.93583	0.009	58.84001	-0.040	59.80821	-0.019	76.81287	-0.022
57.81475	0.003	57.93842	-0.005	58.84210	-0.030	59.81028	-0.029	76.81558	-0.025
57.81734	-0.020	57.93901	-0.016	58.84421	-0.037	59.81238	-0.033	76.81830	-0.027
57.81794	-0.016	57.93961	-0.017	58.84630	-0.031	59.81447	-0.028	76.82102	-0.020
57.81854	-0.011	57.94222	-0.011	58.84840	-0.039	59.81655	-0.033	76.82374	-0.011
57.82113	-0.018	57.94281	-0.018	58.85049	-0.026	59.81865	-0.039	76.82646	-0.018
57.82173	-0.029	57.94341	-0.012	58.85258	-0.026	59.82073	-0.036	76.82919	-0.017
57.82233	-0.009	57.94599	0.004	58.85469	-0.015	59.82283	-0.027	76.83191	-0.013
57.82491	-0.019	57.94659	0.010	58.85679	-0.031	59.82491	-0.034	76.87372	-0.018
57.82551	-0.019	57.94719	0.009	58.85888	-0.034	59.82701	-0.055	76.87644	-0.023
57.82610	-0.005	57.94977	0.027	58.86098	-0.034	59.82910	-0.036	76.87916	-0.006
57.82869	-0.005	57.95038	0.022	58.86307	-0.023	59.83118	-0.037	76.88460	-0.053
57.82929	-0.016	57.95098	0.026	58.86516	-0.037	59.83327	-0.033	76.88733	-0.031
57.82988	-0.014	57.95357	0.033	58.86725	-0.031	59.83535	-0.024	76.89006	-0.027
57.83248	-0.015	57.95417	0.045	58.86934	-0.020	59.83745	-0.017	76.89279	-0.026
57.83308	-0.009	57.95476	0.050	58.87145	-0.031	59.83953	-0.047	76.89552	-0.019
57.83367	-0.013	57.95735	0.086	58.87354	-0.039	59.84161	-0.020	76.89824	-0.031
57.83626	-0.016	57.95794	0.081	58.87565	-0.028	59.84369	-0.028	76.90097	-0.024
57.83686	-0.019	57.95855	0.094	58.87775	-0.032	59.84579	-0.036	76.90369	-0.028
57.83746	-0.013	57.96114	0.095	58.87984	-0.023	59.84788	-0.017	76.90641	-0.005
57.84004	-0.013	57.96174	0.078	58.88192	-0.025	59.84997	-0.040	76.90914	-0.011
57.84065	-0.018	57.96234	0.089	58.88403	-0.026	59.85205	-0.032	76.91186	-0.018
57.84125	-0.031	57.96492	0.114	58.88613	-0.026	59.85415	-0.023	76.91459	-0.014
57.84384	-0.023	57.96552	0.094	58.90394	-0.020	59.85623	-0.036	76.91731	-0.022
57.84444	-0.017	57.96613	0.100	58.90603	-0.038	59.85831	-0.022	76.92003	-0.010
57.84504	-0.012	57.96872	0.116	58.90813	-0.034	59.86039	-0.050	76.92275	-0.014
57.84764	-0.024	57.96932	0.120	58.91023	-0.050	59.86248	-0.032	76.92547	-0.018
57.84823	0.003	57.96992	0.094	58.91233	-0.035	59.93802	-0.060	76.92819	-0.010
57.84883	-0.005	57.97250	0.113	58.91442	-0.031	59.94012	-0.069	76.93092	-0.024
57.85143	-0.018	57.97310	0.100	58.91652	-0.025	59.94221	-0.055	76.93364	-0.011
57.85202	-0.022	57.97371	0.106	58.91862	-0.038	59.94428	-0.059	76.93636	-0.014
57.85262	-0.029	57.97630	0.035	58.92072	-0.037	59.94635	-0.060	76.93909	-0.013
57.85522	-0.032	57.97690	0.091	58.92490	-0.036	59.94845	-0.066	76.94179	-0.012
57.85582	-0.013	57.97749	0.053	58.92699	-0.044	59.95053	-0.069	76.94447	-0.011
57.85642	-0.017	57.98006	0.094	58.92908	-0.022	59.95263	-0.060	76.94717	-0.011
57.85900	-0.013	57.98065	0.072	58.93117	-0.027	59.95471	-0.075	76.94989	-0.005
57.85960	0.000	57.98125	0.050	58.93327	-0.024	59.95680	-0.059	76.95262	-0.015
57.86021	-0.020	57.98381	0.030	58.93536	-0.012	59.95889	-0.057	76.95534	-0.018
57.86280	-0.024	57.98441	0.021	58.93745	-0.060	59.96098	-0.059	76.95806	-0.027
57.86340	-0.012	57.98502	0.032	58.93955	-0.054	59.96307	-0.065	76.96078	-0.028
57.86399	-0.019	57.98761	0.027	58.94762	-0.027	59.96515	-0.064	76.96348	-0.012
57.86657	-0.031	57.98821	0.016	58.94970	-0.016	59.96724	-0.078	76.96621	-0.003
57.86717	-0.014	57.98880	0.000	58.95181	-0.072	59.96933	-0.075	76.96893	-0.013
57.86776	-0.009	58.69591	-0.032	59.65880	-0.037	59.97142	-0.079	76.97166	-0.016
57.87032	-0.022	58.69978	-0.029	59.66089	0.000	59.97351	-0.060	76.97438	-0.019
57.87091	-0.017	58.70187	-0.027	59.66297	-0.064	59.97560	-0.056	76.97710	-0.027
57.87151	-0.015	58.70397	-0.042	59.66507	-0.042	59.97768	-0.056	76.97983	-0.017